Research Article Vol. 1, No. 2 / August 2014 / Optica 119


# Single-shot measurement of the complete temporal intensity and phase of supercontinuum

TSZ CHUN WONG, MICHELLE RHODES,* AND RICK TREBINO

*School of Physics, Georgia Institute of Technology, 837 State Street, Atlanta, Georgia 30332, USA*

**Corresponding author: mrhodes3@gatech.edu*

*Received 25 April 2014; revised 26 June 2014; accepted 28 June 2014 (Doc. ID 210812); published 15 August 2014*

**When a narrowband laser pulse evolves into a broadband pulse, for example, via transmission through a photonic crystal fiber, the resulting continuum usually exhibits massive shot-to-shot pulse-shape fluctuations. The continuum's extreme complexity prevents its single-shot measurement, with the best estimates so far resulting from an average over many pulses. Here we solve this problem using cross-correlation frequency-resolved optical gating, achieving the necessary large spectral range using a polarization-gating geometry and the necessary large temporal range by significantly tilting the reference pulse. Furthermore, we have also discovered that we can simultaneously cancel the previously unavoidable longitudinal geometrical smearing by using a carefully chosen combination of pulse tilt and beam-crossing angle, thus simultaneously achieving the required temporal resolution. We hence make a complete measurement of an individual complex continuum pulse generated in photonic crystal fiber. By enabling measurement of single optical rogue waves, this technique could provide insight and perhaps even lead to the prediction of when mathematically similar, destructive oceanic rogue waves may occur.** 

***OCIS codes:*** (320.0320) Ultrafast optics; (320.7100) Ultrafast measurements.

http://dx.doi.org/10.1364/OPTICA.1.000119

## 1. INTRODUCTION

Supercontinuum (SC) generation is the remarkable nonlinear-optical process by which a narrowband laser pulse efficiently evolves into an extremely broadband pulse [1]. Photonic crystal fiber (PCF) is an especially advantageous medium, conveniently yielding a spatially coherent SC beam [2] and allowing a wide range of applications, including stimulated emission depletion microscopy, optical coherence tomography, optical frequency metrology, and carrier-envelope phase stabilization [3–6].

Interestingly, SC pulses are extremely temporally complex, and trains of them are inherently highly unstable [7–14]. As a result, it has never been possible to measure the temporal intensity and phase of a single SC pulse. Such measurements have been possible if averaged over many pulses, but at best they yield only an estimate of a typical SC pulse [15–21]. At worst, multi-shot measurements of such unstable pulse trains are susceptible to "coherent artifacts" that can mislead the unwary into believing that their pulses are erroneously simple [22,23].

SC measurement recently acquired increased urgency when it was noted (and confirmed) that SC can give rise to optical rogue waves, mathematically equivalent to the oceanic rogue waves that sink dozens of ships every year [24]. Numerical simulations and experimental observations of collections of single-shot spectra have confirmed that SC generation in PCF follows the same L-shaped statistics as oceanic waves, where statistically rare rogue events occur much more often than would be implied by simple Gaussian statistics [25,26]. While the measurement of an oceanic rogue wave is straightforward (if one happens upon such a rare event), its intentional generation is difficult and perhaps also ill-advised (unless on a very small scale). On the other hand, while the generation of an optical rogue wave is simple, routine, and safe, its single-shot complete measurement has remained impossible. Complete

measurements of optical rogue waves could lead to insight into, and eventually to the prediction of, their destructive and difficult-to-simulate oceanic counterparts [26–28].

Unfortunately, the challenges facing single-shot measurement of SC are many. A typical SC generated from PCF is several picoseconds long and has well over 100 nm of spectral bandwidth, easily achieving a time–bandwidth product (TBP) of ~100 or more. Such SC pulses are extremely complex, with fine structure in both the temporal and spectral domains. To further complicate the task, due to the small cores of PCFs, a SC pulse is quite weak, having at most ~20 nJ of energy. Since this energy is spread over a few picoseconds, the intensity of these pulses is also quite low. While addressing one (or occasionally two) of these requirements at a time is now routine, achieving nanojoule sensitivity, large temporal and spectral ranges, and fine temporal and spectral resolution simultaneously on a single shot has not yet been accomplished, despite an ever-increasing need to do so.

Here, we report a general technique that solves this problem. In order to deal with the low energy of the SC pulse, we use a cross-correlation frequency-resolved optical gating (XFROG) setup with a high-energy (regeneratively amplified) reference pulse. This setup provides much more signal and hence sensitivity than a self-referenced nonlinear measurement. Even better, XFROG has been demonstrated to retrieve extremely complicated pulse shapes very reliably [29]. We also chose a polarization-gating (PG) geometry, which has essentially infinite bandwidth and so nicely solves the spectral-width problem immediately. Unfortunately, PG has a drawback: it is a third-order nonlinear process, and therefore, even with a high-intensity reference pulse, it still requires a relatively long (>1 mm) nonlinear medium for adequate signal strength, which will prove problematic for other reasons that we will discuss shortly.

Achieving sufficient temporal range to measure SC is also nontrivial. A typical FROG or XFROG device achieves single-shot measurement by crossing the reference and unknown pulses inside the nonlinear medium at an angle, $\theta$, as depicted in Fig. 1(a). This maps the delay onto the transverse spatial position in the nonlinear medium and also at the camera onto which the nonlinear medium is imaged. The temporal range of the device scales with the crossing angle, and delay ranges up to a few picoseconds are possible with this approach. However, since a delay range of several times the pulse length is necessary, this is not sufficient to measure SC pulses, which are typically longer. An old and well-known innovation that increased the temporal range of autocorrelators to tens of picoseconds was the use of pulse-front tilt (PFT) in the two pulses in the device [30]. We adapt this approach here for XFROG and add PFT, but only to the reference pulse (to avoid potentially distorting the SC). The temporal ranges with and without PFT, $\Delta T_{\mathrm{PFT}}$ and $\Delta T$, are given by (see Fig. 1)

$$\Delta T = \frac{d}{c}\tan\,\theta, \tag{1}$$

$$\Delta T_{\mathrm{PFT}} = \frac{d}{c}\tan(\alpha - \theta), \tag{2}$$

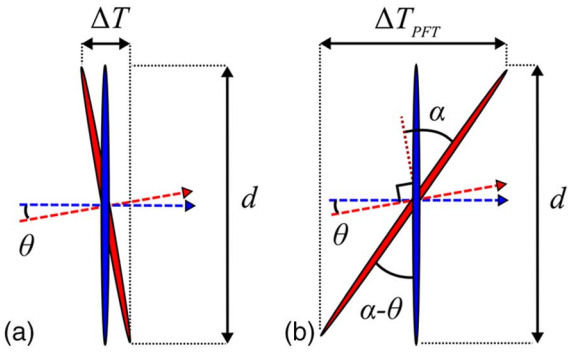


**Fig. 1.** Illustration of the temporal range calculation for single-shot XFROG [see Eqs. (1) and (2)]. (a) Typical device with an untilted reference pulse. The unknown and reference pulses are shown in blue and red, respectively, with arrows showing their propagation directions. The relative delay between the pulses varies transversely, and imaging the beam-crossing region onto a camera achieves single-shot operation. (b) Proposed approach using a reference pulse with pulse-front tilt to increase the temporal range. The tilt angle is $\alpha$.

where $d$ is the beam diameter, $\theta$ is the internal crossing angle, $\alpha$ is the PFT angle, and $c$ is the speed of light. This can easily increase the temporal range by more than an order of magnitude, and hence solves the temporal range problem [31].

The last and most difficult requirement for measuring SC is achieving the required very fine temporal resolution. In a PG geometry (and most other beam geometries as well), this is severely limited by a fundamental effect called longitudinal geometrical smearing (LGS). As the pulses cross in the nonlinear medium, the line of constant delay drifts away from the direction of signal-beam propagation, causing a given camera pixel to see signal light generated from a range of delays, rather than just one delay [32]. The LGS increases with crossing angle at an even faster rate than the temporal range does, significantly limiting the temporal resolution in experiments requiring a large temporal range. In addition, LGS increases with the length of the nonlinear medium, limiting signal strength.

Interestingly, introducing PFT into the gate pulse has a significant impact on LGS, which has not yet been considered in the literature. As shown in the schematic of LGS in a PFT setup [Fig. 2(a)], the zero time delay between the reference and the unknown pulse is located at the centers of both beams at the entrance of the nonlinear medium. Because the signal in a PG geometry follows the same path as the unknown pulse, the spatial center of the signal beam corresponds to different time delays between the pulses as the two beams propagate in different directions. When the signal beam exits the nonlinear medium, the delay between the beams in the center is nonzero. The range of delays contained in the same transverse spatial location, $\delta t_{\mathrm{PFT}}$, is the longitudinal smearing:

$$\delta t_{\mathrm{PFT}} = \frac{L}{c}\left(1 - \frac{\cos\,\alpha}{\cos(\alpha - \theta)}\right), \tag{3}$$

where $L$ is the thickness of the nonlinear medium, $\alpha$ is the PFT angle, $\theta$ is the internal crossing angle, and $c$ is the speed of light.

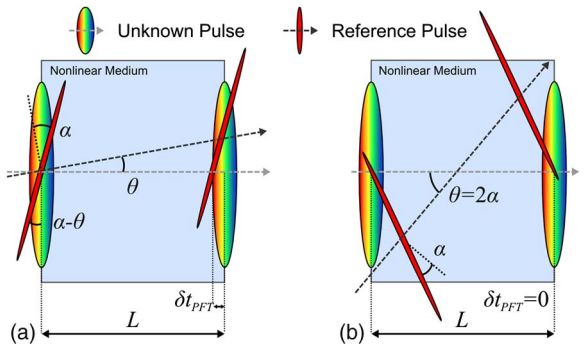


**Fig. 2.** Illustration of longitudinal geometrical smearing in single-shot XFROG. (a) General case with arbitrary internal crossing angle, $\theta$, and PFT angle, $\alpha$. The rectangle with thickness $L$ represents the nonlinear medium. The reference and unknown pulses are shown in red and rainbow colors, respectively, with an arrow indicating their propagation direction. The signal pulse propagates along the same direction as the unknown pulse (the gray dashed line). In this direction, the reference pulse gates the green part (the center) of the unknown pulse at the front of the medium and the red part (the left) of the unknown pulse at the back of the medium. Thus, each transverse position contains signal light created by a range of delays, rather than a single delay. This range is the longitudinal smearing, $\delta t_{\mathrm{PFT}}$. (b) The ideal choice of internal crossing angle, $\theta = 2\alpha$, removes the longitudinal smearing completely while maintaining a large delay range. The reference pulse overlaps with the same part of the unknown pulse at each transverse position throughout the medium. The PFT angle, $\alpha$, here remains the same as in part (a).

Quite fortuitously, from Eq. (3), we find that for a given amount of PFT, a specific internal crossing angle can be chosen that actually perfectly eliminates the LGS. Indeed, Eq. (3) provides two such conditions: $\theta = 0$ and $\theta = 2\alpha$. The solution $\theta = 0$ is not practical in our setup, as it provides for copropagating reference and unknown pulses, which cannot be separated after their interaction inside the nonlinear medium. The second condition, $\theta = 2\alpha$, however, is ideal, and we implement it in our apparatus, thus solving the temporal resolution problem [see Fig. 2(b)]. This condition does not limit flexibility in the temporal range for the device, because the beam size is also a strong factor in determining the overall temporal range. In any case, removing LGS allows the use of a much thicker nonlinear medium (the next limitation on the medium thickness is group-velocity dispersion, which is significantly less restrictive, even for the SC's large spectral width, and can be included in the XFROG retrieval algorithm if desired). And as mentioned above, this also significantly increases the nonlinear interaction length and thus the sensitivity of the device, because the signal pulse energy scales as the square of the nonlinear medium thickness.

Finally, we use a regeneratively amplified reference pulse with 440 μJ of pulse energy, attenuated to just below the threshold for continuum generation in the nonlinear medium in order to maximize the nonlinear–optical interaction without distorting the reference pulse or SC pulse to be measured. This allows our device to measure even extremely weak SC on a single shot. An additional increase in device sensitivity could be achieved by time stretching (chirping) the reference pulse, whose phase is irrelevant in the measurement, so that it overlaps with a larger fraction of the unknown SC pulse. This proved unnecessary in our experiments, but we mention it here in case a weaker SC must be measured.

## 2. METHODS

To create the reference pulse, 80% of the energy from a regenerative amplifier was sent to a 45° polarizer and then to a 600 line/mm diffraction grating. To properly image the diffracted beam, we prefer that the first order diffracts along the normal of the grating surface, setting an incidence angle of 28.7° for 800 nm light. As is shown in Fig. 3, the diffracted beam has PFT because the right side of the pulse hits the grating before the left side of the pulse. This pulse was imaged with 1 : 1 imaging (using a 200 mm lens with 400 mm of propagation before and after) onto the nonlinear medium, 5 mm of BK7. Figure 3 also shows that the beam size is expanded by both the grating and the large incidence angle into the nonlinear medium. The beam expansion combined with the slower phase velocity in the glass causes the PFT angle in the nonlinear medium to be significantly less than the PFT angle in air just after the grating. The tilt angle $\alpha$ in the glass is given by (see Fig. 3)

$$\begin{aligned}\tan\alpha &= (b/n)/(dM(\cos\theta_2/\cos\theta_1))\\ &= \sin\gamma\cos\theta_1/nM\cos\theta_2,\end{aligned} \tag{4}$$

where $b$ is the spatial delay caused by impinging on the grating at incidence angle $\gamma$, $n$ of BK7 is ~1.5, $d$ is the beam diameter at the grating, $M = 1$ is the magnification of the imaging lens, and $\theta_1$ and $\theta_2$ are the incidence and refracted angles, respectively, at the glass surface. We find that the reference pulse had a tilt of ~15° inside the nonlinear medium. It crossed with the SC pulse at an external angle of 43° to satisfy the condition to eliminate LGS. Fine adjustment of the crossing angle of the beams was accomplished by tweaking the angle of the BK7. The beam from the amplifier has a diameter $d$ of about 1 cm. Using Eq. (2), we find that this yields a theoretical temporal range of about 14 ps. The effective temporal range is often less due to the drop-off in intensity in the wings of the beam, but this geometry is sufficient to measure SC pulses 2–3 ps long.

The other 20% of the amplifier pulse was made into a SC seed by spatially and spectrally filtering it (with a filter centered at 785 nm with FWHM 6.5 nm) and then stretching it with

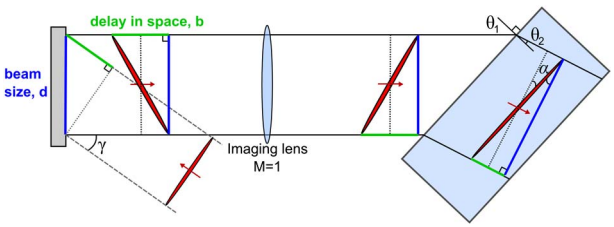


**Fig. 3.** Illustration of how to create PFT and calculate the resulting PFT angle in the nonlinear medium. The PFT angle in glass is smaller than the angle in air after the grating due to the larger size of the refracted beam and the slower phase velocity. The drawing is not to scale, and the angles are slightly exaggerated for clarity.

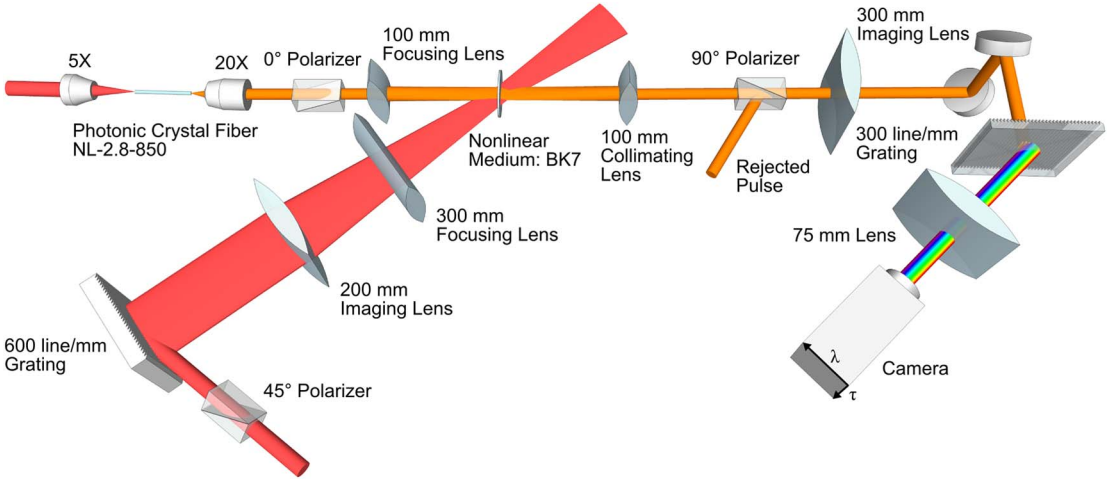


**Fig. 4.** 3D schematic of the experimental apparatus of PG XFROG with PFT in the reference pulse. The red and orange represent the reference pulse and the SC, respectively. The reference pulse gates the SC in the nonlinear medium, which is imaged onto the camera in the vertical direction, mapping time delay to spatial position. The spectrometer consists of a transmission grating and cylindrical lens that generate the spectrum of the gated SC pulse in the horizontal direction.

several centimeters of glass to reduce the peak intensity. It was focused into 23.1 mm of PCF fiber (NL-2.8-850-02, Thorlabs) with a microscope objective and collimated after the fiber with another microscope objective. The spatial profile of the SC was measured by a camera to confirm that it had a single spatial mode. A fiber-coupled spectrometer confirmed the absence of spatial chirp in the SC.

The remainder of our device was a standard single-shot PG XFROG. The experimental setup is shown in Fig. 4. The nonlinear medium was imaged into a simple homemade imaging spectrometer, and the SC pulse gated by the tilted reference pulse was spectrally resolved as a function of delay, yielding an XFROG trace (spectrogram) of the SC. The experimental apparatus had a temporal range (at the camera) of ~8 ps and a spectral range of ~360 nm. Fourier filtering and standard background subtraction were performed before retrieving the intensity and phase with the standard XFROG algorithm.

## 3. RESULTS

The generated SC had 15.5 nJ of energy, and 7.3 nJ was delivered to the nonlinear medium. The measured and retrieved XFROG traces (2048 × 2048 arrays), with a FROG error (rms difference between the measured and retrieved XFROG traces) of 0.85% (indicating good agreement), are shown in Figs. 5(a) and 5(b). The retrieved temporal and spectral intensity and phase are shown in Figs. 5(c) and 5(d). The majority of the measured features are reproduced in the retrieved trace, while the noisy background is appropriately ignored by the XFROG retrieval algorithm. The retrieved spectrum (green solid line) ranged from 715 to 850 nm, showing excellent agreement with an independently measured spectrum (black solid line) from the same SC as was measured by our apparatus. The retrieved spectral peak locations also match well with the measured ones. The duration of the pulse is ~2 ps, and the TBP is ~65. This is, to the best of our knowledge, the first single-shot intensity and phase measurement of SC generated from PCF.

It is important to confirm that our retrieved pulse is correct, but there is no alternative technique available to confirm it. The best that can be done is to compare the spectrum measured by our device with that measured using a standard spectrometer. However, SC generation is an inherently unstable process and suffers from severe shot-to-shot fluctuations, especially in its spectrum. As a result, the only spectrum that can be used to confirm the measurement has to come from the same SC pulse that was measured by the XFROG. Since the SC pulse is extremely weak, sending a sufficient amount of the SC pulse to a spectrometer before the nonlinear medium would greatly reduce the signal strength. Fortunately, in the PG geometry, the signal pulse is generated when the gate pulse

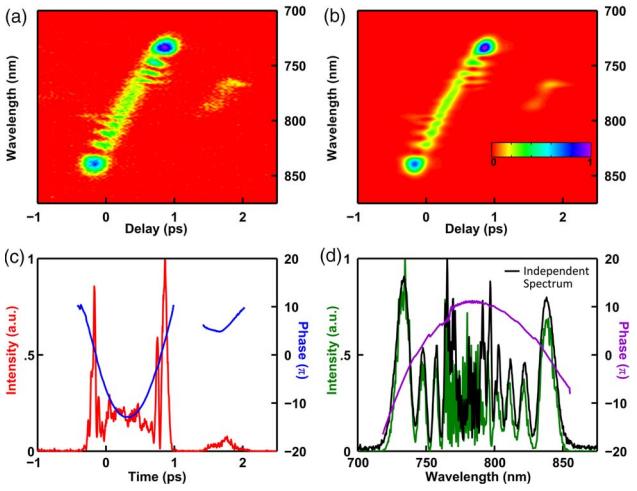


**Fig. 5.** Single-shot PG XFROG measurement of SC generated from a 23.1 mm long NL-2.8-850 photonic crystal fiber. (a) Measured XFROG trace (2048 × 2048 array) after background subtraction, (b) retrieved XFROG trace with rms error of 0.85%, (c) temporal intensity (red) and phase (blue) of the retrieved SC, and (d) spectral intensity (green) and phase (violet) of the retrieved SC with the same-shot spectrum (black).

slightly rotates the polarization of the SC pulse and a polarization analyzer rejects the original, unrotated polarization. Thus, the spectrum of the analyzer-rejected portion of the SC can be independently measured and hence used to confirm the XFROG-measured spectrum on the same shot. So we directed this rejected pulse to pass through the same grating-lens spectrometer as that used for the PG XFROG setup.

When comparing the retrieved spectrum with the same-shot spectrum measured in this manner, we see that the spectral peaks match well at the edges of the spectrum, but there are some small discrepancies in the central region. During the experiment, we found that a small prepulse was ejected from our regenerative amplifier tens of picoseconds before the main pulse. Due to its much lower energy, the prepulse experienced only slight spectral broadening in the PCF and contributed to the spectrum from 760 to 800 nm, with a FWHM of 15 nm. As FROG is a time-gating device, and the prepulse precedes the gating reference pulse by many picoseconds, the prepulse does not affect the recorded FROG trace. A spectrometer, however, integrates over all the energy that impinges onto the sensor during its exposure time. Thus, the same-shot spectrum is affected by a prepulse, while the FROG measurement is not. A correction to the spectrum was performed by first capturing a FROG trace of the prepulse at the correct delay, determining its spectrum, and then subtracting this spectrum from the same-shot spectrum. This assumes incoherent addition of the prepulse spectrum and the SC spectrum, which is not precisely the case, but it is not possible to do better. We believe that this accounts for the discrepancies in the central region of the spectrum.

With our device demonstrated to accurately measure pulses, we measured a very different SC pulse generated using a seed with less applied chirp and slightly larger energy, sent into a longer piece of fiber 32.2 mm long. The resulting SC had longer temporal duration, broader spectral bandwidth, and less pulse energy. The measured and retrieved XFROG traces (2048 × 2048 array), with a FROG error of 0.57%, are shown in Figs. 6(a) and 6(b). The retrieved temporal and spectral intensity and phase are shown in Figs. 6(c) and 6(d). The retrieved pulse has a TBP of ~96 with a duration of ~2.5 ps and spectrum ranging from 590 to 800 nm. The broader spectrum is not surprising, as the seed is less chirped and hence has a higher peak intensity, which usually generates a SC with a larger bandwidth. The temporal and spectral phases from Figs. 6(c) and 6(d) show more quadratic phase in the output, which is expected because the spectral bandwidth is larger and the fiber is longer. The same-shot spectrum was not measured, as the previous measurement demonstrated the validity of this measurement technique.

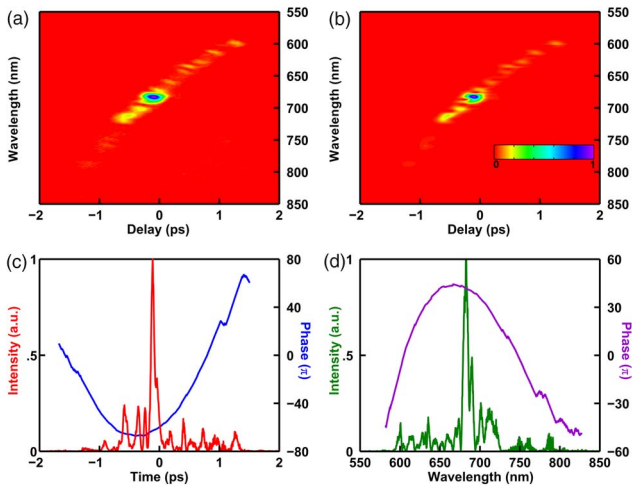


**Fig. 6.** Single-shot PG XFROG measurement of SC generated from a 32.2 mm long NL-2.8-850 photonic crystal fiber. (a) Measured XFROG trace (2048 × 2048 array) after background subtraction, (b) retrieved XFROG trace with a G-error of 0.57%, (c) temporal intensity (red) and phase (blue) of the retrieved SC, and (d) spectral intensity (green) and phase (violet) of the retrieved SC.

## 4. CONCLUSIONS

To summarize, we have proposed and demonstrated the use of PFT in the reference arm of PG XFROG to measure the intensity and phase of SC generated from PCF on a single shot. The unlimited phase-matching bandwidth of the PG geometry achieves the required large bandwidth. Further, introducing PFT into the reference pulse increases the temporal range of the single-shot device. More importantly, controlling the internal crossing angle between the tilted reference pulse and the SC inside the nonlinear medium eliminates the longitudinal geometrical smearing completely and allows the use of a thick nonlinear medium to achieve nanojoule sensitivity in our device. As regenerative amplifiers routinely achieve kilohertz repetition rates, and camera frame rates and data storage are more likely to limit the data collection rate, the apparatus described here is more than sufficient for studies of optical rogue waves involving many millions of pulses. Our method is easily able to adapt to different bandwidth and temporal range requirements imposed by optical rogue waves. For example, the optical rogue waves identified by Solli *et al.* require a temporal range of ~6 ps and a spectral bandwidth of ~300 nm centered at 1064 nm [25]. Our current apparatus is capable of such a measurement once the mirrors, lenses, and gratings are replaced with those appropriate for the shifted center wavelength.

## FUNDING INFORMATION

National Science Foundation (NSF) (ECCS-1028825).

## REFERENCES

1. R. R. Alfano and S. L. Shapiro, "Emission in the region 4000 to 7000 Å via four-photon coupling in glass," Phys. Rev. Lett. **24**, 584–587 (1970).
2. J. K. Ranka, R. S. Windeler, and A. J. Stentz, "Visible continuum generation in air-silica microstructure optical fibers with anomalous dispersion at 800 nm," Opt. Lett. **25**, 25–27 (2000).
3. D. Wildanger, E. Rittweger, L. Kastrup, and S. W. Hell, "STED microscopy with a supercontinuum laser source," Opt. Express **16**, 9614–9621 (2008).
4. G. Humbert, W. Wadsworth, S. Leon-Saval, J. Knight, T. Birks, P. St. J. Russell, M. Lederer, D. Kopf, K. Wiesauer, E. Breuer, and D. Stifter, "Supercontinuum generation system for optical coherence

tomography based on tapered photonic crystal fibre," Opt. Express **14**, 1596–1603 (2006).
5. T. Udem, R. Holzwarth, and T. W. Hansch, "Optical frequency metrology," Nature **416**, 233–237 (2002).
6. D. J. Jones, S. A. Diddams, J. K. Ranka, A. Stentz, R. S. Windeler, J. L. Hall, and S. T. Cundiff, "Carrier-envelope phase control of femtosecond mode-locked lasers and direct optical frequency synthesis," Science **288**, 635–639 (2000).
7. H. Kubota, K. R. Tamura, and M. Nakazawa, "Analyses of coherence-maintained ultrashort optical pulse trains and supercontinuum generation in the presence of soliton-amplified spontaneous-emission interaction," J. Opt. Soc. Am. B **16**, 2223–2232 (1999).
8. A. L. Gaeta, "Nonlinear propagation and continuum generation in microstructured optical fibers," Opt. Lett. **27**, 924–926 (2002).
9. J. M. Dudley, G. Genty, and S. Coen, "Supercontinuum generation in photonic crystal fiber," Rev. Mod. Phys. **78**, 1135–1184 (2006).
10. B. Wetzel, A. Stefani, L. Larger, P. A. Lacourt, J. M. Merolla, T. Sylvestre, A. Kudlinski, A. Mussot, G. Genty, F. Dias, and J. M. Dudley, "Real-time full bandwidth measurement of spectral noise in supercontinuum generation," Sci. Rep. **2**, 882 (2012).
11. U. Møller, S. T. Sørensen, C. Jakobsen, J. Johansen, P. M. Moselund, C. L. Thomsen, and O. Bang, "Power dependence of supercontinuum noise in uniform and tapered PCFs," Opt. Express **20**, 2851–2857 (2012).
12. S. T. Sørensen, C. Larsen, U. Møller, P. M. Moselund, C. L. Thomsen, and O. Bang, "Influence of pump power and modulation instability gain spectrum on seeded supercontinuum and rogue wave generation," J. Opt. Soc. Am. B **29**, 2875–2885 (2012).
13. S. T. Sørensen, C. Larsen, U. Møller, P. M. Moselund, C. L. Thomsen, and O. Bang, "The role of phase coherence in seeded supercontinuum generation," Opt. Express **20**, 22886–22894 (2012).
14. T. Godin, B. Wetzel, T. Sylvestre, L. Larger, A. Kudlinski, A. Mussot, A. Ben Salem, M. Zghal, G. Genty, F. Dias, and J. M. Dudley, "Real time noise and wavelength correlations in octave-spanning supercontinuum generation," Opt. Express **21**, 18452–18460 (2013).
15. Q. Cao, X. Gu, E. Zeek, M. Kimmel, R. Trebino, J. Dudley, and R. S. Windeler, "Measurement of the intensity and phase of supercontinuum from an 8-mm-long microstructure fiber," Appl. Phys. B **77**, 239–244 (2003).
16. J. Dudley, X. Gu, L. Xu, M. Kimmel, E. Zeek, P. O'Shea, R. Trebino, S. Coen, and R. Windeler, "Cross-correlation frequency resolved optical gating analysis of broadband continuum generation in photonic crystal fiber: simulations and experiments," Opt. Express **10**, 1215–1221 (2002).
17. X. Gu, M. Kimmel, A. Shreenath, R. Trebino, J. Dudley, S. Coen, and R. Windeler, "Experimental studies of the coherence of microstructure-fiber supercontinuum," Opt. Express **11**, 2697–2703 (2003).
18. X. Gu, L. Xu, M. Kimmel, E. Zeek, P. O'Shea, A. P. Shreenath, R. Trebino, and R. S. Windeler, "Frequency-resolved optical gating and single-shot spectral measurements reveal fine structure in microstructure-fiber continuum," Opt. Lett. **27**, 1174–1176 (2002).
19. D. Lee, P. Gabolde, and R. Trebino, "Toward single-shot measurement of a broadband ultrafast continuum," J. Opt. Soc. Am. B **25**, A34–A40 (2008).
20. J. Liu, Y. Feng, H. Li, P. Lu, H. Pan, J. Wu, and H. Zeng, "Supercontinuum pulse measurement by molecular alignment based cross-correlation frequency resolved optical gating," Opt. Express **19**, 40–46 (2011).
21. B. Tsermaa, B.-K. Yang, M.-W. Kim, and J.-S. Kim, "Characterization of supercontinuum and ultraviolet pulses by using XFROG," J. Opt. Soc. Korea **13**, 158–165 (2009).
22. M. Rhodes, G. Steinmeyer, J. Ratner, and R. Trebino, "Pulse-shape instabilities and their measurement," Laser Photon. Rev. **7**, 557–565 (2013).
23. J. Ratner, G. Steinmeyer, T. C. Wong, R. Bartels, and R. Trebino, "Coherent artifact in modern pulse measurements," Opt. Lett. **37**, 2874–2876 (2012).
24. M. Hopkin, "Sea snapshots will map frequency of freak waves," Nature **430**, 492 (2004).
25. D. R. Solli, C. Ropers, P. Koonath, and B. Jalali, "Optical rogue waves," Nature **450**, 1054–1057 (2007).
26. J. M. Dudley, G. Genty, and B. J. Eggleton, "Harnessing and control of optical rogue waves in supercontinuum generation," Opt. Express **16**, 3644–3651 (2008).
27. N. Akhmediev, A. Ankiewicz, J. M. Soto-Crespo, and J. M. Dudley, "Rogue wave early warning through spectral measurements?" Phys. Lett. A **375**, 541–544 (2011).
28. D. R. Solli, C. Ropers, and B. Jalali, "Active control of rogue waves for stimulated supercontinuum generation," Phys. Rev. Lett. **101**, 233902 (2008).
29. L. Xu, E. Zeek, and R. Trebino, "Simulations of frequency-resolved optical gating for measuring very complex pulses," J. Opt. Soc. Am. B **25**, A70–A80 (2008).
30. R. Wyatt and E. E. Marinero, "Versatile single-shot background-free pulse duration measurement technique, for pulses of subnanosecond to picosecond duration," Appl. Phys. **25**, 297–301 (1981).
31. T. C. Wong and R. Trebino, "Single-frame measurement of complex laser pulses tens of picoseconds long using pulse-front tilt in cross-correlation frequency-resolved optical gating," J. Opt. Soc. Am. B **30**, 2781–2786 (2013).
32. R. Trebino, *Frequency-Resolved Optical Gating: the Measurement of Ultrashort Laser Pulses* (Kluwer Academic, 2002).